

# Electrostatic Spacecraft Collision Avoidance Using Piece-Wise Constant Charges

Shuquan Wang and Hanspeter Schaub

Simulated Reprint from

## Journal of Guidance, Control, and Dynamics

Volume 33, Number 2, Mar.–Apr., 2010, Pages 510–520, DOI:10.2514/1.44397



*A publication of the*  
American Institute of Aeronautics and Astronautics, Inc.  
1801 Alexander Bell Drive, Suite 500  
Reston, VA 22091

# Electrostatic Spacecraft Collision Avoidance Using Piece-Wise Constant Charges

Shuquan Wang\* and Hanspeter Schaub†

This paper develops a three-phase piece-wise constant spacecraft charge maneuver to achieve a short-range collision avoidance with a symmetric relative trajectory. This symmetric trajectory guarantees collision avoidance, restores the original relative motion direction, and keeps the relative kinetic energy level the same as the initial one. The paper first presents an analytical solution to calculate a unique symmetric trajectory when the middle phase is a circular trajectory. Next a general symmetric trajectory programming strategy is developed where the middle-phase can be any conic section. Four constraints are required to guarantee a symmetric collision avoidance trajectory, while five independent variables are required to solve the problem. This leaves one degree of freedom which is utilized to optimize the trajectory subject to specific cost charge functions. There is a duality in the charge solution when solving for the open-loop trajectory with one of the solutions being false. This is addressed by properly initializing and confining the region of the numerical search routine. Minimum charge criteria are determined to avoid a collision by analyzing the geometric properties of the two-body system and comparing the results from circular transitional trajectory calculations.

## I. Introduction

Clustered spacecraft have many advantages over a single large monolithic satellite. However, spacecraft cluster concepts also introduce the issue of potential collisions. In close-proximity spacecraft missions, such as close formations and small satellite swarms, the chance for spacecraft to collide must be treated carefully to prevent the huge cost of an unexpected collision. Collisions can occur when some spacecraft within the cluster have control or sensor failures, or are lacking in their guidance strategy to guarantee collision avoidance among a large number of cluster members. For long-term formation flying missions, a collision can also occur when the influences of the orbital disturbances accumulate. The chance of a potential collision from multiple sources motivates the studies of the spacecraft collision avoidance problem.

The most common approach in dealing with spacecraft collision avoidance is to examine the collision probability of a spacecraft cluster and perform some velocity corrections to reduce the probability to an acceptable level. Patera and Peterson develop a method to select a maneuver that will reduce the collision probability.<sup>1</sup> This method minimizes the maneuver magnitude and space vehicle propellant expenses. Slater et al.<sup>2</sup> use the available state and disturbance information to calculate the actual probability of collision based on a probabilistic model, then discuss the velocity correction requirements to avoid collisions. Patera proposes a spherical conflict volume to calculate the conflict probability in identifying high-risk conjunctions.<sup>3</sup> The conflict probabilities are larger than associated collision probabilities and therefore are more easily interpreted. All of the above works use thrusters to achieve the velocity corrections. These strategies use propellant, which will increase the fuel budget of the spacecraft. Further, the associated exhaust plume impingement may cause damage to the instruments on board in a close proximity formation.

In this paper a different scenario is considered where an active Coulomb control strategy is used after a potential collision has been detected. The craft are assumed to be moving within dozens of meters from each other, and the relative velocities are small—on the order of centimeters per second. This collision avoidance strategy is not applicable to rapidly approaching spacecraft because of the technical challenges of achieving sufficiently large electrostatic fields. Instead, this work assumes fields that are comparable to the electrostatic potentials that can occur naturally with geostation-

ary spacecraft. Here the potentials can reach multiple kV levels.<sup>4</sup> The collision avoidance maneuver strategy uses only piece-wise constant electrostatic (Coulomb) forces. Coulomb thrusting can generate the required micro- and milli-newton levels of forces to avoid a collision of two slowly drifting spacecraft while requiring essentially no propellant and a few watts of electrical power.

The concept of Coulomb thrusting or Coulomb Formation Flying (CFF) is first introduced by King et al. in Reference 4. CFF uses Coulomb forces to control the distances between spacecraft to achieve the desired relative motion. Spacecraft will naturally charge to either positive or negative voltages due to their interaction with the local space plasma environment. The spacecraft charge level can be actively controlled by continuously emitting electrons or ions as used on the current CLUSTER mission.<sup>5,6</sup> The fuel-efficiency of Coulomb thrusting is at least 3–5 orders greater than that of Electric Propulsion (EP), and typically requires only a few watts of electrical power to operate.<sup>4</sup> A challenge of CFF is that, unlike conventional thrusters that can produce a thrust vector in any direction, the Coulomb forces lie only along the line-of-sight directions between spacecraft. But this is less of an issue in using Coulomb forces to avoid a collision. The most important factor in preventing collision is the separation distance, which can be fully controlled using Coulomb forces. Another challenge of CFF is that the sparse space plasma will shield electrostatic charges. This effect will reduce the amount of electrostatic force that a neighboring charged spacecraft will experience. The amount of shielding is characterized by the Debye length.<sup>7,8</sup> At separation distances greater than a Debye length the perceived inter-craft Coulomb force quickly becomes negligible. At LEO where the plasma is relatively dense and cold, the Debye length is on the order of centimeters. This results in a strong shielding of Coulomb forces and makes Coulomb thrusting not feasible. However, at GEO the Debye lengths range between 100–1000 meters.<sup>4,9</sup> At 1 AU in deep space the Debye length ranges around 20–50 meters.<sup>4</sup> This makes the Coulomb thrusting concept feasible for HEO and deep space missions while the minimum separation distances are less than 100 meters.

The CFF concept has been investigated for several different mission scenarios. Lappas et al. in Reference 10 develop a hybrid propulsion strategy by combining Coulomb forces and standard electric thrusters for formation flying on the orders of tens of meters in GEO. Reference 11 analyses the stability of a spinning two-craft Coulomb tether. It shows that, if the Debye length is larger than the separation distance then the nonlinear radial motion is locally stable, otherwise the radial motion is unstable. And the perturbed out-of-plane motion is always stable regardless of Debye length. Vasavada and Schaub<sup>12</sup> present analytical tools to determine the

\* Graduate Research Assistant, Aerospace Engineering Sciences Department, University of Colorado at Boulder, AIAA student member.

† Associate Professor, Aerospace Engineering Sciences Department, University of Colorado at Boulder, H. Joseph Smead Fellow, AIAA Associate Fellow.

Presented as Paper 09-184 at the 19<sup>th</sup> AAS/AIAA Space Flight Mechanics Meeting, Savannah, GA, Feb. 9–12, 2009. Copyright ©2009 by Shuquan Wang. Published by the American Institute of Aeronautics and Astronautics, Inc. with permission.

charge solution for a static four-craft formation. Reference 13 designs a two-stage charge feedback control strategy for a 1-D constrained Coulomb structure. It also analyses the condition for symmetric relative motions of Coulomb structure to be stabilizable by investigating the total energy of the system. Hussein and Schaub derive the collinear three-craft spinning family of solutions in Reference 14. A feedback control based on the linearized model is designed to stabilize a collinear virtual Coulomb tether system. Asymptotic stability is achieved if the system's angular momentum is equivalent to the estimated/nominal angular momentum, which is utilized to calculate the nominal charges. However, none of these CFF related works consider the issue of performing active collision avoidance. Such a capability will be required when considering flying larger numbers of craft in close proximity.

Reference 15 is the first publication that develops a collision avoidance strategy using only Coulomb forces. A controller is designed based on Lyapunov stability analysis and requires only feedback on separation distance. Without charge saturations the controller can prevent any collision. Considering charge saturations, the paper finds the analytical criteria for an avoidable collision by assuming the Debye length to be infinity. While this feedback control strategy can maintain specified safety separation distances, this control will cause the craft to depart in a different direction from when the collision avoidance maneuver started. This change in direction should be avoided if possible to not re-direct the craft and cause them to approach another craft.

Instead of designing a feedback control strategy, this paper investigates an open-loop strategy to find a symmetric trajectory to achieve the collision avoidance objective. In particular, a solution is sought that retains the original relative velocity vector after the collision avoidance maneuver. The paper investigates how to develop such open-loop charged relative motion trajectories. How to feedback stabilize such a trajectory and make it robust to unmodeled dynamics and sensor errors is the topic of future work. Such a feedback strategy is non-trivial due to the under-actuated nature of the Coulomb force. For example, the line-of-sight force cannot change the momentum vector to reverse an overshoot. Assuming the Debye length to be large compared to the separation distance, and that the spacecraft charges are piece-wise constant, the relative equations of motion during a constant charge phase have exactly the same algebraic form as in the Gravitational 2-Body Problem (G2BP). In this work the spacecraft are assumed to be operating in deep space and not orbiting a gravitational body. Thus, the relative trajectory segments corresponding to constant spacecraft charge result in a conic sections.<sup>16</sup> By switching the spacecraft charges, a symmetric trajectory made of three patched conic sections, repel-attract-repel, is sought to achieve a collision avoidance meanwhile to retain the relative speed magnitude and direction. The geometries of the symmetric trajectories are explored to investigate charge optimality of the resulting open-loop maneuvers. This is important when the limited charge capability of actual craft are taken into consideration. Further, given a maximum charging capability, initial condition criteria that lead to a successful collision avoidance maneuver are explored.

## II. Problem Statement

### A. Charged Spacecraft Equations of Motion

This paper considers two spacecraft free-flying in 3-dimensional space where there are no external forces acting on the system. The scenario of the two body system is shown in Figure 1. Assuming point-charge models for the spacecraft, the partially-shielded electrostatic potential generated by the  $i^{\text{th}}$  spacecraft in a plasma environment is given by<sup>17</sup>

$$V_i(r) = k_c \frac{q_i}{r} \exp(-r/\lambda_d), \quad (1)$$

where  $k_c = 8.99 \times 10^9 \text{ C}^{-2} \cdot \text{N} \cdot \text{m}^2$  is the Coulomb constant,  $q_i$  is the charge of the  $i^{\text{th}}$  spacecraft,  $r$  is the separation distance between the  $i^{\text{th}}$  spacecraft and the point of interest,  $\lambda_d$  is the Debye length which characterizes the strength of the plasma shielding effect. The corresponding electrostatic field is obtained by taking the gradient

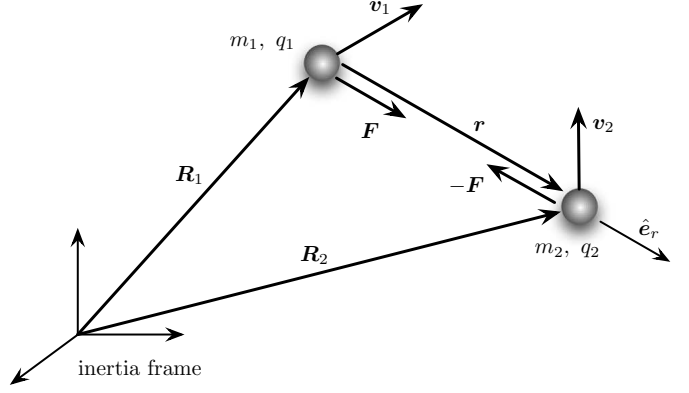


Figure 1: Illustration of the 2-spacecraft system.

of the potential:

$$E_i(\mathbf{r}) = -\nabla_r V_i(r) = k_c \frac{q_i}{r^2} \left(1 + \frac{r}{\lambda_d}\right) \exp\left(-\frac{r}{\lambda_d}\right) \hat{e}_r, \quad (2)$$

where  $\mathbf{r}$  is the inertial position vector pointing from the  $i^{\text{th}}$  spacecraft to the point of interest,  $\hat{e}_r$  is the unit vector of  $\mathbf{r}$ . Thus, the Coulomb force between the two spacecraft, acting on  $m_1$ , is

$$\begin{aligned} \mathbf{F} &= q_1 E_2(\mathbf{r}_{21}) = k_c \frac{q_1 q_2}{r^2} \left(1 + \frac{r}{\lambda_d}\right) \exp\left(-\frac{r}{\lambda_d}\right) \hat{e}_{21} \\ &= -k_c \frac{q_1 q_2}{r^2} \left(1 + \frac{r}{\lambda_d}\right) \exp\left(-\frac{r}{\lambda_d}\right) \hat{e}_{12}, \end{aligned} \quad (3)$$

where  $\mathbf{r}_{12}$  is the relative position vector from spacecraft 1 (SC1) to spacecraft 2 (SC2),  $\hat{e}_{12}$  is the unit vector of  $\mathbf{r}_{12}$ . In the remaining context, we use  $\hat{e}_r$  to represent  $\hat{e}_{12}$  for brief notation. From the expression of the Coulomb force, it can be seen that the smaller the plasma Debye length, the shorter the effective range of a given electrical charge. For high Earth orbits the Debye length ranges between 100–1000 m.<sup>4,18,9</sup> In deep space at 1 AU distance from the sun the Debye length can vary between 30–50 m. CFF typically has spacecraft separation distances less than 100 m.

The inertial equations of motion (EOM) of the two charged spacecraft are

$$m_1 \ddot{\mathbf{R}}_1 = -k_c \frac{q_1 q_2}{r^2} \left(1 + \frac{r}{\lambda_d}\right) \exp\left(-\frac{r}{\lambda_d}\right) \hat{e}_r, \quad (4a)$$

$$m_2 \ddot{\mathbf{R}}_2 = k_c \frac{q_1 q_2}{r^2} \left(1 + \frac{r}{\lambda_d}\right) \exp\left(-\frac{r}{\lambda_d}\right) \hat{e}_r, \quad (4b)$$

where  $\mathbf{R}_i$  is the inertial position vector of the  $i^{\text{th}}$  spacecraft. The inertial relative acceleration vector  $\ddot{\mathbf{r}}$  is

$$\begin{aligned} \ddot{\mathbf{r}} &= \ddot{\mathbf{R}}_2 - \ddot{\mathbf{R}}_1 \\ &= \frac{k_c q_1 q_2}{m_1 m_2 r^2} (m_1 + m_2) \left(1 + \frac{r}{\lambda_d}\right) \exp\left(-\frac{r}{\lambda_d}\right) \hat{e}_r. \end{aligned} \quad (5)$$

Note that these equations do not explicitly consider planetary gravity and the Lorentz forces acting on the spacecraft. Pollock et. al. prove that the Lorentz force magnitude is not comparable with the Coulomb force in GEO.<sup>19</sup> If the collision avoidance maneuver time is very small compared to the cluster orbital period, then Eq. (5) can also be considered as an approximation of the charged relative orbital motion. For example, a GEO spacecraft collision avoidance maneuver that takes minutes would be very short compared to the 1 day orbit period, and thus the relative orbital motion would have a secondary effect on the relative motion.

This paper finds a symmetric patched conic section trajectory to prevent a collision, while forcing the departure velocity vector to be the same as the initial arrival velocity vector. Reference 16 shows that if  $\lambda_d \rightarrow \infty$ , and the charge product  $Q = q_1 q_2$  is constant,

then the relative motion trajectory of the two spacecraft is a conic section. Letting  $\lambda_d \rightarrow \infty$  and defining

$$\mu = -k_c \frac{Q(m_1 + m_2)}{m_1 m_2}, \quad (6)$$

Eq. (5) is rewritten as

$$\ddot{\mathbf{r}} = -\frac{\mu}{r^3} \mathbf{r}. \quad (7)$$

Eq. (7) has exactly the same algebraic form as the EOM of the G2BP. If the charge product  $Q$  is constant, then the effective gravitational coefficient  $\mu$  is also constant. Thus, the resulting motion can be described by a conic section. Note that here  $\mu$  can be positive or negative. The negative and constant charge product results in a positive effective gravitational constant  $\mu > 0$ . In this case, Eq. (7) is exactly the same as the G2BP. If  $Q$  is negative and constant, then the relative trajectory is a repulsive hyperbola, where SC2 is moving along a hyperbola, and SC1 stays at the farther focus point.<sup>16</sup> If the charge product  $Q$  is piece-wise constant, then the relative trajectory would be a patched conic section.

### B. 3-Phase Symmetric Trajectory Scenario

For a two spacecraft system controlled only by Coulomb forces, generally there is an infinity of possible charge and charge switching time solutions which achieve a collision avoidance. This paper investigates a symmetric trajectory programming approach to avoid a collision as well as to hold the relative velocity.

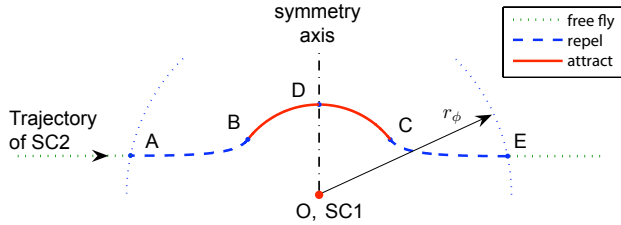


**Figure 2: Illustration of the symmetric patched conic section trajectory with respect to SC1.**

An example of the symmetric relative trajectory scenario is shown in Figure 2. The controlled part of the symmetric trajectory is composed of three phases: repel–attract–repel. At the beginning, the two spacecraft are flying freely and approaching each other such that their minimum separation distance will violate a desired safety distance  $r_s$ . At the point  $A$ , the separation distance  $r$  between the spacecraft reaches a potential collision region range  $r_\phi$ . The spacecraft are charged such that  $Q > 0$  and the spacecraft start to repel each other to avoid the collision. The magnitude of the charge product is held constant in Phase-I until point  $B$  is reached. Thus the trajectory  $\widehat{AB}$  is a repulsive hyperbola. At point  $B$  the charge product switches to a negative value such that the spacecraft are attracting each other. During Phase-II from the point  $B$  to the point  $C$ , the charge product is again held constant. The arc  $\widehat{BC}$  is an attractive conic section which can be ellipsis, parabola, or hyperbola depending on the relative arrival velocity magnitude. At the point  $C$  the charge product switches back to the same value as in arc  $\widehat{AB}$  to produce a symmetric trajectory to  $\widehat{AB}$ . At the point  $E$ , the spacecraft are discharged and begin to fly freely in space. The entire trajectory is symmetric about the axis  $\overline{OD}$ . The symmetry axis  $\overline{OD}$  is the line crossing SC1 and perpendicular to the initial relative velocity.

From the above description of the 3-phase trajectory, it can be seen that the trajectory is determined by the three-charge product during the three phases, and the two-charge switching time at the points  $B$  and  $C$ . Once these five variables are determined, the relative trajectory is determined.

### III. Circular Transitional Orbit Programming

Before studying the general symmetric trajectories, let us at first investigate a special case where the Phase-II trajectory is a section

of a circle as illustrated in Figure 3. Assume that the relative position vector  $\mathbf{r}_A$  and the relative velocity  $\dot{\mathbf{r}}_A$  at the point  $A$  can be measured. There are five unknown parameters that need to be determined: the three charge products  $Q_I$ ,  $Q_{II}$  and  $Q_{III}$ , and the two charge switching times at points  $B$  and  $C$ . To solve for these five variables some constraints must be clarified.

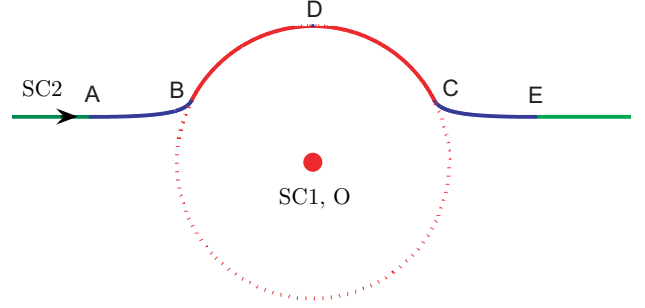


**Figure 3: Scenario of the circular Phase-II trajectory.**

#### A. Constraints

For Phase-I  $\widehat{AB}$  and Phase-III  $\widehat{CE}$  to be symmetric, the charge products should be the same value. Thus, the first constraint is

$$Q_{III} = Q_I. \quad (8)$$

Because the trajectory of Phase-II  $\widehat{BC}$  is a section of a circle, its shape is always symmetric about the symmetry axis  $\overline{OD}$ . Then a symmetric arc  $\widehat{BC}$  requires that the angle  $\angle DOC$  satisfies

$$\angle DOC = \angle BOD. \quad (9)$$

The point  $B$  connects Phase-I and Phase-II. Thus  $\dot{\mathbf{r}}_B$  must be perpendicular to  $\mathbf{r}_B$  because Phase-II is circular. This implies the point  $B$  is the periapsis of Phase-I. This results in the third constraint:

$$r_B = r_{pl}. \quad (10)$$

The trajectory of Phase-II is a section of a circle, this requirement can be formulated using the angular momentum magnitude:

$$h_{II}^2 = \mu_{II} r_B. \quad (11)$$

The collision avoidance task requires that the separation distance  $r(t)$  must be greater than a certain safe-restraint distance  $r_s$  for all time:

$$r(t) \geq r_s. \quad (12)$$

This constraint is global and comes from the collision avoidance mission. For the convenience of calculation, this safety constraint is expressed by the condition

$$r_{\min} = \gamma r_s, \quad (13)$$

where  $\gamma \geq 1$ . In the case that Phase-II is a section of a circle,  $r_{\min} = r_B$ . Thus the final safety constraint for a circular transitional symmetric trajectory is

$$r_B = \gamma r_s. \quad (14)$$

Now five constraints given in Eqs. (8)–(11) and (14) have been found.

#### B. Circular Transitional Orbit Algorithm

The symmetric constraint in Eq. (8) provides  $Q_{III}$  once  $Q_I$  is obtained. Note that the angle  $\angle DOC$  is the true anomaly angle (in case the point  $D$  is the periapsis) of Phase-II. Once the conic section properties of Phase-II, which are determined by  $Q_{II}$ , are achieved, the charge switching time at the point  $C$  is then solved by using Kepler's equation and the symmetry constraint in Eq. (9).

Now there are three variables  $(Q_I, Q_{II}, t_I)$  left out of the five unknown parameters that still need to be determined. The conic section properties of Phase-I are solved using  $\mathbf{r}_A$  and  $\dot{\mathbf{r}}_A$ . The eccentricity vector of Phase-I is

$$\mathbf{c}_I = \dot{\mathbf{r}}_A \times \mathbf{h} - \frac{\mu_I}{r_A} \mathbf{r}_A, \quad (15)$$

where  $r_A = |\mathbf{r}_A|$ ,  $\mathbf{h} = \mathbf{r}_A \times \dot{\mathbf{r}}_A$  is the specific angular momentum of the system, and

$$\mu_I = -k_c \frac{Q_I(m_1 + m_2)}{m_1 m_2} \quad (16)$$

is the effective gravitational coefficient of Phase-I. Note that, through Eq. (6), finding the charge products  $Q_I$  and  $Q_{II}$  is equivalent to finding  $\mu_I$  and  $\mu_{II}$ . The vector  $\mathbf{h}$  is constant by the assumption that there are no external forces acting on the system. The eccentricity and semi-major axis of Phase-I are calculated by

$$e_I = -\frac{\|\mathbf{c}_I\|}{\mu_I}, \quad (17a)$$

$$a_I = \frac{r_A \mu_I}{2\mu_I - r_A v_A^2}, \quad (17b)$$

where  $v_A = \|\dot{\mathbf{r}}_A\|$  is the magnitude of the relative velocity vector. The angle  $\angle AOD$  is calculated as

$$\angle AOD = \arctan\left(\frac{h}{r_A v_A}\right) - \frac{\pi}{2}. \quad (18)$$

Utilizing the constraint that the point  $B$  must be the periapsis of Phase-I, the charge switching time  $t_B$  at point  $B$  is calculated via

$$t_B = \frac{|N_{AI}|}{\sqrt{\mu_I/a_I}} \quad (19)$$

with the right hand side of this equation being completely determined by  $\mu_I$ , which in return is determined by  $Q_I$ . Thus, it can be concluded that the Phase-I trajectory are determined by the charge product  $Q_I$ .

The radius  $r_B$  is calculated by

$$r_B = \frac{h^2/\mu_I}{1 - e_I}, \quad (20)$$

where the eccentricity  $e_I$  is given by Eq. (17a). Substituting Eq. (20) into the safety constraint in Eq. (14) and multiplying both sides by  $\mu_I(1 - e_I)/(\gamma r_s)$ , yields

$$\mu_I(1 - e_I) = \frac{h^2}{\gamma r_s}. \quad (21)$$

Subtracting both sides by  $\mu_I$ , taking the square of both sides, and using  $e_I = -\frac{\|\mathbf{c}_I\|}{\mu_I} = \left\| \frac{\mathbf{r}_A}{r_A} - \frac{\dot{\mathbf{r}}_A \times \mathbf{h}}{\mu_I} \right\|$ , yields

$$\mu_I^2 e_I^2 = \mu_I^2 - 2\mu_I \dot{\mathbf{r}}_A \times \mathbf{h} \cdot \mathbf{r}_A / r_A + \dot{\mathbf{r}}_A \times \mathbf{h} \cdot \dot{\mathbf{r}}_A \times \mathbf{h}. \quad (22)$$

Substituting Eq. (22) into Eq. (21), yields

$$-2\mu_I \dot{\mathbf{r}}_A \times \mathbf{h} \cdot \mathbf{r}_A / r_A + \dot{\mathbf{r}}_A \times \mathbf{h} \cdot \dot{\mathbf{r}}_A \times \mathbf{h} = \frac{h^4}{\gamma^2 r_s^2} - \frac{2\mu_I h^2}{\gamma r_s}. \quad (23)$$

Thus, the Phase-I effective gravitational coefficient for a circular transitional trajectory is solved by grouping terms containing  $\mu_I$ :

$$\mu_{I,c} = \frac{1}{2} \frac{\frac{h^4}{\gamma^2 r_s^2} - \dot{\mathbf{r}}_A \times \mathbf{h} \cdot \dot{\mathbf{r}}_A \times \mathbf{h}}{\frac{h^2}{\gamma r_s} - \dot{\mathbf{r}}_A \times \mathbf{h} \cdot \frac{\mathbf{r}_A}{r_A}}. \quad (24)$$

After obtaining  $\mu_{I,c}$ , the variable  $t_I$  is determined by Eq. (19). These values of  $\mu_I$  and  $t_I$  ensure that at the point  $B$  the relative

speed vector is perpendicular to the relative position vector, meanwhile the safety constraint  $r_B = \gamma r_s$  is also satisfied.

The next step is to find a proper  $Q_{II}$  or  $\mu_{II}$  that results in a circular orbit. Using the constraint for a circular transitional orbit in Eq. (11),  $\mu_{II}$  is found to be

$$\mu_{II,c} = \frac{h^2}{r_B} = \frac{h^2}{\gamma r_s}. \quad (25)$$

To find the Phase-II duration time  $t_{II}$ , the Phase-II symmetry constraint in Eq. (9) is utilized. Note that the angular velocity is constant in Phase-II, the duration time is proportional to the angle  $\angle BOC$  as:

$$t_{II,c} = \angle BOC \cdot \frac{T_{II}}{2\pi} = 2\angle BOD \cdot \frac{T_{II}}{2\pi} = \frac{\angle BOD \cdot T_{II}}{\pi}, \quad (26)$$

where the period of the Phase-II circular orbit is  $T_{II} = \sqrt{\mu_{II}/r_{II}^3}$ , the angle  $\angle BOD$  is given by

$$\angle BOD = \angle AOD - |f_{AI}| = \angle AOD + \text{atan}\left(\frac{\hat{\mathbf{i}}_{cI} \times \hat{\mathbf{i}}_{rA} \cdot \hat{\mathbf{i}}_h}{\hat{\mathbf{i}}_{cI} \cdot \hat{\mathbf{i}}_{rA}}\right), \quad (27)$$

where  $\hat{\mathbf{i}}_{cI}$ ,  $\hat{\mathbf{i}}_{rA}$  and  $\hat{\mathbf{i}}_h$  are the unit vectors of  $\mathbf{c}_I$ ,  $\mathbf{r}_A$  and  $\mathbf{h}$  respectively. The angle  $\angle AOD$  is expressed in Eq. (18).

Thus a symmetric trajectory with Phase-II being a part of a circular orbit has been found. Specifically, the variables  $\mu_I$ ,  $\mu_{II}$ ,  $Q_{III}$ ,  $t_B$ ,  $t_{II}$  are calculated through Eqs. (24), (25), (8), (19) and (26), respectively. Note that this circular transitional trajectory solution is calculated analytically.

#### IV. General Symmetric Trajectory Programming Strategy

After solving a circular Phase-II trajectory in the last section, this section investigates the more general symmetric collision avoidance trajectory with the Phase-II trajectory being any type of conic section.

A general 3-phase symmetric trajectory is shown in Figure 2. As mentioned in the last section, as with the circular Phase-II case, there are five unknowns that need to be determined:  $[Q_I, Q_{II}, Q_{III}, t_B, t_{II}]$ .

##### A. Constraints

The general constraints are largely the same as those for the circular transitional orbit. The three constraints in Eqs. (8), (9), and (13) are directly used to ensure a symmetric trajectory. Because here the Phase-II trajectory is a part of a general conic section, the circular constraints in Eqs. (10) and (11) are not applicable.

Since the arc  $\widehat{BC}$  does not necessarily be a part of a circle, for Phase-II to be symmetric about the axis  $\widehat{OD}$ , the point  $D$  must be the periapsis or apoapsis of Phase-II. This requirement is formulated as:

$$r_D = r_{p,II}, \quad \text{or} \quad r_D = r_{a,II}, \quad (28)$$

where  $r_{p,II}$  and  $r_{a,II}$  are the periapsis radius and the apoapsis radius of Phase-II.

Now there are four equality constraints to solve the patched conic collision avoidance trajectory. Eqs. (8), (9) and (28) are from the symmetric patched conic section properties and ensure a symmetric trajectory. The constraint given by Eq. (14) is required by the collision avoidance task. To complete the 5-variable searching problem, one more constraint is needed.

Note that the four equality constraints ensure a collision avoidance trajectory and meanwhile result in a symmetric trajectory. The remaining one degree of freedom actually provides a flexibility in solving for the five variables. Here this section assumes that a proper value of  $Q_I$  is given, then constructs a closed-loop numerical iteration routine to find other four variables. This iteration routine can be used as a part of the charge-optimal trajectory programming algorithm that updates  $Q_I$  such that a certain charge cost function is minimized. The charge-optimization examples are shown and discussed in the second simulation case in the numerical simulation section.

## B. General Numerical Iteration Routine

Assuming that a proper value of  $Q_I$  has been given, this section develops a numerical iteration routine to find a symmetric patched conic section trajectory to avoid a potential collision. The charge product  $Q_I$  and the initial conditions  $[r_A, \dot{r}_A]$  determine the conic section of Phase-I. Without loss of generality, assume that  $t_A = 0$ . If  $t_B$  is given, the angle  $\angle AOB$  can be calculated using Kepler's equation in Phase-I. The states  $[r_B, \dot{r}_B]$  are determined by solving the orbit EOM of Phase-I. Utilizing the constraint that the point  $D$  must be the periapsis or apoapsis of Phase-II, the point  $C$  is determined by the constraint in Eq. (9). Phase-III is determined by the state of point  $C$ , which can be inferred from  $t_B$ . Thus, the charge switching time  $t_B$  logically determines the whole patched conic section trajectory. In the numerical iteration routine,  $t_B$  is chosen as the variable to be propagated.

Now  $t_B$  has been chosen as the variable to be propagated in the iteration loop. Given an initial guess of  $t_B$ , it is updated according to the error of a target function. The states at the point  $B$  are determined by using the conic section properties of Phase-I. The mean hyperbolic anomaly of the point  $B$  considered in Phase-I is calculated using the Kepler's equation:

$$N_{B1} = N_{A1} + \sqrt{\frac{\mu_1}{a_1^3}} \cdot t_B = N_{A1} + n_1 \cdot t_B. \quad (29)$$

Then the hyperbolic anomaly  $H_{B1}$  is calculated by numerically solving the standard anomaly relationship:<sup>20</sup>

$$N_{B1} = e_1 \sinh(H_{B1}) + H_{B1}. \quad (30)$$

Thus the true anomaly of the point  $B$  in Phase-I is determined by

$$f_{B,1} = 2 \cdot \arctan \left( \tanh \left( \frac{H_{B1}}{2} \right) \sqrt{\frac{e_1 + 1}{e_1 - 1}} \right). \quad (31)$$

The radius and the magnitude of the relative velocity at the point  $B$  are

$$r_B = \frac{h^2 / \mu_1}{1 - e_1 \cos f_{B1}}, \quad (32a)$$

$$v_B = \sqrt{\mu_1 \left( \frac{2}{r_B} - \frac{1}{a_1} \right)}, \quad (32b)$$

where  $h$  is the magnitude of the specific angular momentum determined by the initial conditions. Eq. (32b) is obtained from the energy equation.

After obtaining the relative motion states at point  $B$ , Phase-II is determined by the symmetric conic section constraints. Specifically, the charge product  $Q_{II}$  and the point  $C$  are determined through the following process. At first, the angle  $\angle AOB$  is calculated by

$$\angle AOB = |f_{B,1} - f_{A,1}|. \quad (33)$$

The angle  $\angle BOD$  is determined by the geometry relation:

$$\angle BOD = \angle AOD - \angle AOB. \quad (34)$$

According to the symmetric constraint in Eq. (9), the angle

$$\angle COD = \angle BOD \quad (35)$$

is solved. Thus the point  $C$  is located. Note that of the five variables that determine the symmetric conic section trajectory, the points  $B$ ,  $C$ , and the charge products  $Q_I$ ,  $Q_{III}$  have been solved. The only variable left to be determined is the charge product  $Q_{II}$ . Solving for  $\mu$  from Eq. (7) yields

$$\mu_{II} = -k_c \frac{Q_{II}(m_1 + m_2)}{m_1 m_2}. \quad (36)$$

Once  $\mu_{II}$  is solved,  $Q_{II}$  is also determined. The following development solves for  $\mu_{II}$  based on the states of the point  $B$  and the symmetric constraints.

Since the arc  $\widehat{BC}$  is a part of a conic section, it has all of the properties of conic section orbit. Utilizing the vis-viva equation, the eccentricity  $e$  is expressed as:

$$e = \sqrt{1 + \left( \frac{v^2}{\mu} - \frac{2}{r} \right) \frac{h^2}{\mu}}. \quad (37)$$

Because  $h$  is assumed to be constant, the expression of the eccentricity in Eq. (37) contains only three unknown variables  $r$ ,  $v$  and  $\mu$ . Substituting Eq. (37) into the radius equation, yields

$$r = \frac{h^2}{\mu + \cos f \sqrt{\mu^2 + \left( v^2 - \frac{2\mu}{r} \right) h^2}}. \quad (38)$$

Transforming Eq. (38) to separate the square root term, yields

$$\cos f \sqrt{\mu^2 + \left( v^2 - \frac{2\mu}{r} \right) h^2} = \frac{h^2}{r} - \mu. \quad (39)$$

Squaring Eq. (39) and using the fact that  $1 - \cos^2 f = \sin^2 f$ , Eq. (39) is simplified to be

$$\sin^2 f \mu^2 - \frac{2h^2}{r} \sin^2 f \mu - \cos^2 f v^2 h^2 + \frac{h^4}{r^2} = 0. \quad (40)$$

This equation contains four variables  $\mu$ ,  $f$ ,  $r$  and  $v$ . Note that Eq. (40) is valid for all conic section orbits. Evaluating  $f$ ,  $r$  and  $v$  at point  $B$  in Phase-II, Eq. (40) becomes a quadratic equation of  $\mu$ . The values for  $r_B$  and  $v_B$  are given by Eq. (32). By the symmetry constraint, the point  $D$  can only be the periapsis or apoapsis of Phase-II. If the point  $D$  is the periapsis, then

$$f_{B,II} = -\angle BOD. \quad (41)$$

Otherwise  $D$  is the apoapsis of Phase-II with

$$f_{B,II} = \pi - \angle BOD. \quad (42)$$

In both cases, the resulting final equations after substituting  $f_{B,II}$  into Eq. (40) are identical:

$$\underbrace{\sin^2 \angle BOD}_{l_1} \mu_{II}^2 - \underbrace{\frac{2h^2}{r_B} \sin^2 \angle BOD}_{l_2} \mu_{II} - \underbrace{\cos^2 \angle BOD v_B^2 h^2 + \frac{h^4}{r_B^2}}_{l_3} = 0. \quad (43)$$

Analytically solving for  $\mu_{II}$  from Eq. (43), the charge product in Phase-II is then obtained by Eq. (36).

Note that given  $\mu_1$ ,  $t_B$  and  $\angle BOD$ , generally there are two solutions of  $\mu_{II}$  to Eq. (43):

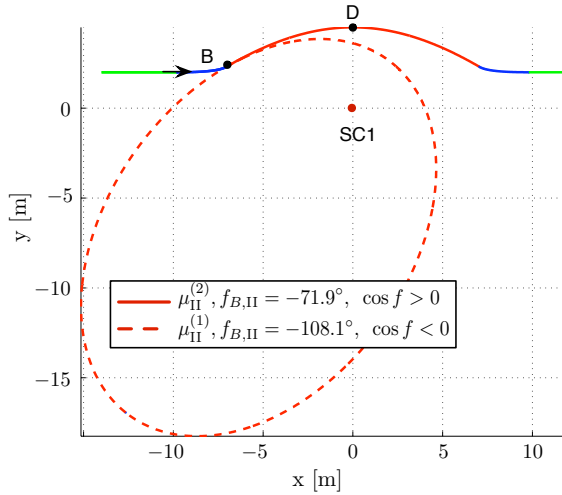
$$\mu_{II}^{(1)} = \frac{h^2}{r_B} + \frac{1}{2 \sin^2 \angle BOD} \sqrt{l_2^2 - 4l_1 l_3}, \quad (44a)$$

$$\mu_{II}^{(2)} = \frac{h^2}{r_B} - \frac{1}{2 \sin^2 \angle BOD} \sqrt{l_2^2 - 4l_1 l_3}. \quad (44b)$$

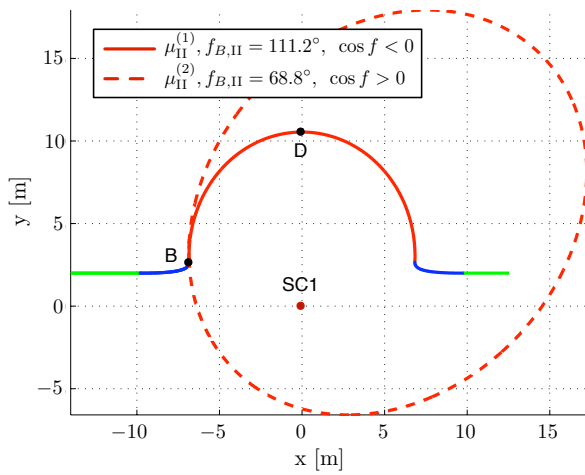
Substituting Eq. (44) into the RHS of Eq. (39), yields

$$\frac{h^2}{r} - \mu = \mp \frac{1}{2 \sin^2 \angle BOD} \sqrt{l_2^2 - 4l_1 l_3}. \quad (45)$$

This indicates that the two solutions result in two opposite signs in the RHS of Eq. (39). But for a particular value of  $f$ , either  $-\angle BOD$  or  $\pi - \angle BOD$ , the LHS of Eq. (39) must have a specific sign. This means only one of the two solutions to Eq. (43) satisfies Eq. (39). In other words, only one of the two values in Eq. (44) results in a symmetric trajectory.



a) Point  $D$  is the periapsis of Phase-II.



b) Point  $D$  is the apoapsis of Phase-II.

**Figure 4:** Two cases of using  $\mu_{II}^{(1,2)}$  solutions, in both cases only one of the two solutions results in an actual symmetric trajectory.

The plots in Figure 4 show the two scenarios using  $\mu_{II}^{(1,2)}$  given by Eq. (44). Figure 4(a) shows the case that the point  $D$  is expected to be the periapsis of Phase-II. Figure 4(b) shows the case that the point  $D$  is designated as the apoapsis of Phase-II. In Figure 4(a), the angle  $\angle BOD = 71.9^\circ$ , and  $f_{B,II}$  is expected to be  $-\angle BOD = -71.9^\circ$ . With this value of  $f_{B,II}$ , the LHS of Eq. (39) must be positive. Correspondingly, only  $\mu_{II}^{(2)}$  satisfies Eq. (39). This is confirmed by Figure 4(a). Figure 4(b) confirms the other case that only  $\mu_{II}^{(1)}$  results in the symmetric trajectory with the point  $D$  being the apoapsis of Phase-II.

By assuming that the variables  $Q_I$  and  $t_B$  are given, the previous development outlines how to solve for the states at the points  $B$  and  $C$ , and the charge product of Phase-II  $Q_{II}$ . However, in our present algorithm  $t_B$  is not explicitly determined. Note that three constraints have been used in deriving the formulas in Eqs. (8), (28), and (9). The safety constraint in Eq. (13) needs to be implemented to achieve a collision avoidance trajectory. A numerical search routine is expected to find an appropriate  $t_B$  such that the closest distance  $r_{\min} = \gamma r_s$ , where  $\gamma \geq 1$ .

The following theorem provides a rule to find the minimum distance in the whole trajectory.

**Theorem 1** Consider the 3-Phase symmetric patched conic section trajectory as shown by Figure 2. If the point  $D$  is the periapsis of Phase-II, then the minimum distance of the entire  $\widehat{AE}$  trajectory

is the periapsis radius of Phase-II, i.e.:

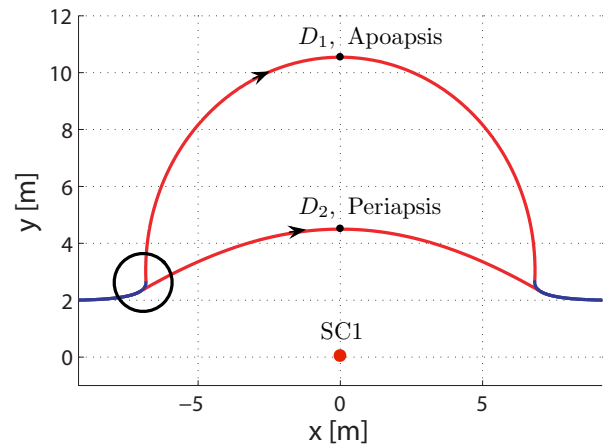
$$r_{\min} = r_{p,II} \quad (46)$$

If the point  $D$  is the apoapsis of Phase-II, then the minimum distance is the periapsis radius of Phase-I, i.e.:

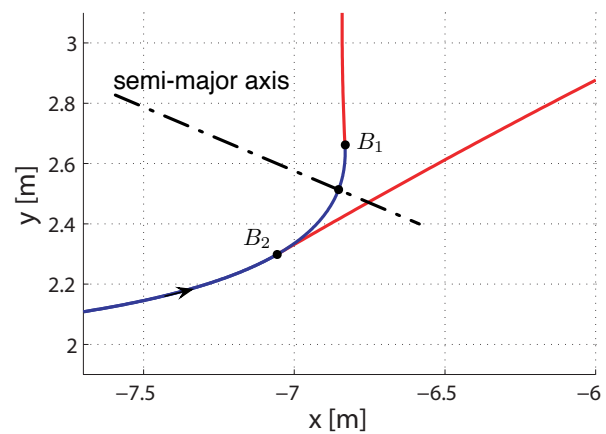
$$r_{\min} = r_{p,I} \quad (47)$$

**Proof** If  $D$  is the periapsis of Phase-II, then  $r_{p,II}$  is the minimum distance in Phase-II. So it's true that  $r_{p,II} < r_B$ . Because  $\angle BOD < 90^\circ$ ,  $f_{B,II} \in (-90^\circ, 0^\circ)$ , thus  $\dot{r}_B < 0$ . Then the periapsis of Phase-I does not lie along the arc  $\widehat{AB}$ . This indicates that throughout Phase-I,  $\dot{r} < 0$ . Thus,  $r_B$  is the minimum distance in Phase-I. Because  $r_{p,II} < r_B$ ,  $r_{p,II}$  is the minimum distance in the entire trajectory.

If  $D$  is the apoapsis of Phase-II, then  $r_B$  is the minimum distance in Phase-II because  $f_{B,II} \in (90^\circ, 180^\circ)$  and  $\dot{r}_B > 0$ . Note that if  $\dot{r}_A \leq 0$ , then the periapsis of Phase-I must lie in the arc  $\widehat{AB}$  because  $\dot{r}$  crosses zero in Phase-I. So  $r_{p,I}$  is the minimum distance in Phase-I, which indicates that  $r_{p,I} < r_B$ . Because  $r_B$  is the minimum distance in Phase-II,  $r_{p,I}$  is the minimum distance in the entire trajectory.  $\square$



a) Big scenario.



b) Focused on Phase-I & Phase-II connecting points.

**Figure 5:** Illustration of the two cases with the point  $D$  being the periapsis and apoapsis of Phase-II.

The proof of Theorem 1 indicates that if the point  $D$  is the periapsis of Phase-II, then  $t_B < t_{p,I}$  where  $t_{p,I}$  is the time for SC2 to fly from the point  $A$  to the periapsis of Phase-I. If point  $D$  is the apoapsis of Phase-II, then  $t_B > t_{p,I}$ . Figure 5(b) illustrates this scenario in detail. Figure 6 shows the change of  $r_{p,II}$  w.r.t.  $t_B$  assuming that  $\mu_I$  is fixed. It can be seen that when  $t_B < t_{p,I}$

and  $\mu_{II}^{(2)}$  is used,  $r_{p,II}$  is monotonically increasing as  $t_B$  increases; when  $t_B > t_{p,I}$  and  $\mu_{II}^{(1)}$  is used,  $r_{p,II}$  is monotonically decreasing as  $t_B$  increases. Thus, a symmetric collision avoidance trajectory with the point  $D$  being the periapsis of Phase-II can be solved by initializing  $t_B^{(0)} < t_{p,I}$  and updating  $t_B$  using a common numerical methods such as Newton's method or the secant method.

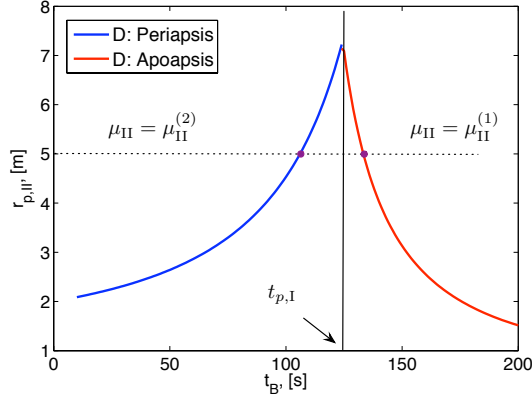


**Figure 6:** Given  $\mu_I$ , the resulting  $r_{p,II}$  with respect to  $t_B$ .

Alternatively initializing  $t_B^{(0)} > t_{p,I}$  and using  $\mu_{II}^{(1)}$  lead to a symmetric collision avoidance trajectory with the point  $D$  being the apoapsis of Phase-II. In this case, by setting  $r_{p,I} = \gamma r_s$  and solving for corresponding  $\mu_I$  from Eq. (24), any symmetric solution of Phase-II trajectory will satisfy the collision avoidance requirement. Thus, there are infinite choices of  $t_B$  that lead to symmetric maneuvers if the point  $D$  is the apoapsis of Phase-II.

Before performing a numerical search for  $t_B$  under a given  $\mu_I$ , it must be decided a priori whether a periapsis or an apoapsis  $D$  point solution is being sought. During the numerical iterations the current estimates of  $t_B$  must be constrained to remain either larger or smaller than  $t_{p,I}$ . If  $t_B$  crosses  $t_{p,I}$  without switching the  $\mu_{II}$  solution, the algorithm will lead to an asymmetric trajectory with  $f_{B,II}$  lying in a wrong quadrant, as shown by the dashed lines in Figure 4.

Note that the path with the point  $D$  being the apoapsis of Phase-II is a longer path, both in length and in time. Practically speaking, there is a bigger chance for the longer path to be influenced by disturbances. Though in developing the algorithm the Debye length effect is not taken into consideration, this effect does exist in the space environment. Thus, the shorter path with the point  $D$  being the periapsis is preferred.

Finally, all the required sub-steps have been presented to outline the overall collision avoidance algorithm. The basic logic is to search for a proper  $t_B^*$  such that the collision avoidance criteria

$$r_{p,II} = \gamma r_s \quad (48)$$

is satisfied, with the point  $D$  being the periapsis of Phase-II. In this paper, Newton's method is used in the numerical searching for  $t_B^*$  such that the following target function becomes zero:

$$g(t_B) = r_{p,II}(t_B) - \gamma r_s. \quad (49)$$

The iteration routine to determine a symmetric collision avoidance with  $D$  being the periapsis of Phase-II propagates according to the following steps:

**Step 1 Initialization:** From the measurements  $\mathbf{r}_A$  and  $\dot{\mathbf{r}}_A$ , calculate  $e_I$ ,  $a_I$  through Eq. (17), and calculate the angle  $\angle AOD$  through Eq. (18). Prescribe a proper  $\mu_I$ , which means  $|\mu_I|$  must be greater than  $|\mu_{I,c}|$  to ensure  $r_{p,I} > \gamma r_s$ . It must also make sure  $Q_I$  is implementable, which means  $Q_I < Q_{\max}$ . Calculate  $t_{p,I}$ . Initialize  $t_B$ :

$$t_B^{(0)} = \alpha t_{p,I} \quad (50)$$

where  $0 < \alpha < 1$ .

- Step 2** Solve for the point  $B$ 's states  $r_B$  and  $v_B$  through Eqs. (29)–(32).
- Step 3** Solve for  $\mu_{II}^{(2)}$  by Eq. (44), using the minus sign. Calculate  $r_{p,II}$  through

$$r_{p,II} = a_{II}(1 - e_{II}) \quad (51)$$

and  $a_{II}$  is solved by the energy equation,  $e_{II}$  is calculated through Eq. (37) evaluating at point  $B$  in Phase-II.

**Step 4** Calculate  $g(t_B)$  by Eq. (49). Judge whether  $|g(t_B)| < \text{Tol}$ . If yes, **STOP**. Otherwise, go to **Step 5**. Here Tol is the tolerance of the iteration error in the unit of meters. This paper uses Tol =  $10^{-4}$  m in the numerical simulations.

**Step 5** Calculate  $g' = \frac{\partial g}{\partial t_B}$  using the finite difference method.

**Step 6** Update  $t_B^{(i+1)} = t_B^{(i)} - \frac{g}{g'}$ ,  $i = i + 1$ . Go to **Step 2**.

After choosing a proper value of  $Q_I$ , this routine calculates a symmetric collision avoidance trajectory composed of three patched conic-sections.

## V. Collision Avoidance Criteria with Charge Saturation

The previous section develops a numerical routine to find a symmetric patched conic section trajectory to avoid the collision and meanwhile preserve the relative velocity magnitude and direction of the two-spacecraft system. In deriving this routine, it is assumed that the charge product of the two spacecraft is unlimited. If the charge product limitation is taken into consideration, the system's ability to avoid a potential collision is then limited. Under certain conditions, for example the two spacecraft are approaching each other too quickly, the collision would be unpreventable. This section determines the criteria to predict whether a potential collision can be prevented using the presented collision avoidance routines.

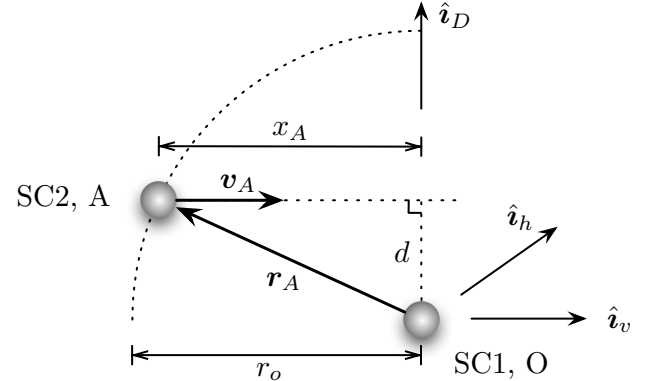


**Figure 7:** Geometry of the 2-spacecraft system.

Figure 7 illustrates the geometry of the two spacecraft system when the collision avoidance strategy is triggered at time  $t_A$ . The vectors  $\mathbf{r}_A$ ,  $\mathbf{v}_A$  and  $\mathbf{h}$  can be expressed in the  $\{\hat{i}_v, \hat{i}_h, \hat{i}_D\}$ <sup>1</sup> frame as

$$\mathbf{r}_A = -x_A \hat{i}_v + d \hat{i}_D \quad (52a)$$

$$\mathbf{v}_A = v_0 \hat{i}_v \quad (52b)$$

$$\mathbf{h} = \mathbf{r}_A \times \mathbf{v}_A = dv_0 \hat{i}_h \quad (52c)$$

<sup>1</sup> $\{\hat{i}_v, \hat{i}_h, \hat{i}_D\}$  centers at SC1, with  $\hat{i}_v$  pointing to the SC2's relative velocity direction,  $\hat{i}_h$  is the unit vector of the relative angular momentum,  $\hat{i}_D$  closes the right hand coordinate.

This section is investigating the critical state with  $\gamma = 1$ . Substituting Eq. (52) into Eq. (24) and using the fact  $\|r_A\| = r_\phi$ , yield

$$\mu_{1,c} = \frac{r_\phi v_0^2 d^2 - r_s^2 r_\phi v_0^2}{2r_s(r_\phi - r_s)} \quad (53)$$

Eq. (53) provides the value of  $\mu_1$  that results in  $r_{p,1} = r_s$ . Thus, the circular transitional orbit solution gives  $\mu_1$  in the critical state.

**Theorem 2** Consider a repulsive hyperbola motion governed by Eq. (7), with  $\mu < 0$  being constant. Given initial position and velocity  $[r_0, \dot{r}_0]$ , the radius of the periapsis  $r_p$  increases as  $|\mu|$  increases.

**Proof** To mathematically prove this theorem, it's required to express  $r_p$  in terms of  $\mu$  and initial conditions. For a repulsive hyperbola, the periapsis radius is given as<sup>16</sup>

$$r_p = a(1 + e) \quad (54)$$

Here  $a$  and  $e$  are actually determined by the initial conditions and  $\mu$ . Substituting  $e = \sqrt{1 - h^2/\mu a}$  and Eq. (17b) into Eq. (54) and using  $|\mu| = -\mu$  instead of  $\mu$ , yields

$$r_p = \frac{1}{2|\mu|/r_0 + v_0^2} \left( |\mu| + \sqrt{|\mu|^2 + h^2(2|\mu|/r_0 + v_0^2)} \right) \quad (55)$$

where  $r_0 = \|r_0\|$ ,  $v_0 = \|\dot{r}_0\|$ ,  $h = \|r_0 \times \dot{r}_0\|$ , which are all determined by the initial conditions.

It's still not obvious to see the trend of  $r_p$  as  $|\mu|$  increases. Taking a partial derivative of  $r_p$  with respect to  $|\mu|$ , yields

$$\frac{\partial r_p}{\partial |\mu|} = \frac{1 + (|\mu| + h^2/r_0)/\beta}{2|\mu|/r_0 + v_0^2} - \frac{|\mu| + \beta}{r_0(2|\mu|/r_0 + v_0^2)^2} \quad (56)$$

where  $\beta = \sqrt{|\mu|^2 + h^2(2|\mu|/r_0 + v_0^2)}$ . The trend of  $r_p$  as  $\mu$  increases is determined by the sign of  $\frac{\partial r_p}{\partial |\mu|}$ . Eq. (56) can be changed to be:

$$\frac{\partial r_p}{\partial |\mu|} = \frac{1}{(2|\mu|/r_0 + v_0^2)^2} \left\{ \frac{|\mu|}{r_0} + v_0^2 + \left( \frac{|\mu|^2}{r_0} + |\mu|v_0^2 \right) / \beta \right\} \quad (57)$$

Eq. (57) gives a simplified expression of  $\frac{\partial r_p}{\partial |\mu|}$  with every individual term being positive. Thus, the partial derivative  $\frac{\partial r_p}{\partial |\mu|}$  is always positive. This proves that  $r_p$  increases as  $|\mu|$  increases.  $\square$

Applying Theorem 2 in the 3-phase symmetric patched conic section scenario yields the following lemma.

**Lemma 1** For the 3-Phase patched conic section scenario as shown in Figure 2, the circular transitional trajectory solution provides the minimum value of  $Q_1$  that satisfies the collision avoidance constraint  $r_{\min} \geq r_s$ .

**Proof** For the critical case where  $\gamma = 1$ , the circular transitional trajectory has the following properties:

$$r_{p,1} = r_s, \quad r_{II} = r_s \quad (58)$$

where  $r_{II}$  is the radius of Phase-II, which is constant.

By Theorem 2,  $\mu_{1,c}$  in Eq. (53) provides the minimum value of  $|\mu_1|$  that satisfies  $r_{p,1} \geq r_s$ . From Eq. (6), the charge product  $Q_1$  is proportional to  $|\mu_1|$ , thus the circular transitional trajectory provides the minimum value of  $Q_1$  such that  $r_{p,1} \geq r_s$ . For Phase-II, the radius is equal to  $r_s$ , which satisfies the collision avoidance requirement. So the circular transitional trajectory solution provides the minimum  $Q_1$  to avoid the collision.  $\square$

**Theorem 3** For the two effective gravitational coefficients given by Eq. (24) and Eq. (25),  $\mu_{1,c} > |\mu_{II,c}|$  if and only if  $d < d^* = r_s \sqrt{\frac{r_\phi}{3r_\phi - 2r_s}}$ .

**Proof** First, let us investigate  $\mu_{II,c} - |\mu_{1,c}|$ :

$$\begin{aligned} \mu_{II,c} - |\mu_{1,c}| &= \mu_{II,c} + \mu_{1,c} \\ &= \frac{h^2}{r_s} + \frac{r_\phi v_0^2 d^2 - r_s^2 r_\phi v_0^2}{2r_s(r_\phi - r_s)} \\ &= \frac{v_0^2}{2r_s(r_\phi - r_s)} \left( (3r_\phi - 2r_s)d^2 - r_\phi r_s^2 \right) \end{aligned} \quad (59)$$

When  $|\mu_{1,c}| > \mu_{II,c}$ ,  $\mu_{II,c} - |\mu_{1,c}| < 0$ , applying this to the formula in Eq. (59), yields

$$\begin{aligned} \frac{v_0^2}{2r_s(r_\phi - r_s)} \left( (3r_\phi - 2r_s)d^2 - r_\phi r_s^2 \right) < 0 \\ \Leftrightarrow d < \sqrt{\frac{r_\phi r_s^2}{3r_\phi - 2r_s}} = d^* \end{aligned} \quad (60)$$

$\square$

Theorem 2 and Lemma 1 show  $Q_1$  is lower bounded by the circular Phase-II solution:

$$Q_1 \geq Q_{1,c} = -\frac{\mu_{1,c} m_1 m_2}{k_c(m_1 + m_2)} = -\frac{(r_\phi v_0^2 d^2 - r_s^2 r_\phi v_0^2) m_1 m_2}{2k_c r_s (r_\phi - r_s)(m_1 + m_2)} \quad (61)$$

If  $d$  satisfies the condition in Theorem 3, then the circular transfer orbit provides the minimum charge product level among all the collision avoidance solutions. To illustrate this, consider the following numerical simulation results with the initial conditions:

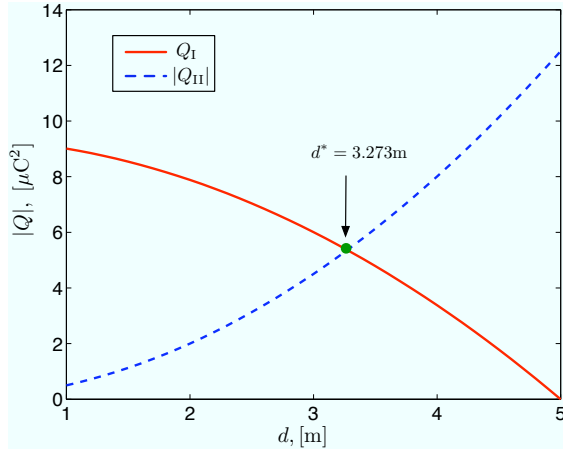
$$\begin{aligned} \mathbf{R}_1(t_0) &= [0, 0, 0]^T \text{ m}, \quad \dot{\mathbf{R}}_1(t_0) = [0, 0, 0]^T \text{ m/s}, \\ \mathbf{R}_2(t_0) &= [20, d, 0]^T \text{ m}, \quad \dot{\mathbf{R}}_2(t_0) = [-0.03, 0, 0]^T \text{ m/s} \end{aligned} \quad (62)$$

and with  $r_\phi = 15$  m,  $r_s = 5$  m. Figure 8 shows the charge product magnitudes under different values of the offset distance  $d$ . For the circular transitional trajectory case Theorem 3 states that  $Q_1 > Q_{II}$  when  $d < 3.2733$  m, and this is reflected in Figure 8(a). Because the minimum magnitude of  $Q_1$  is given by the circular transitional trajectory solution, the circular transitional trajectory solution gives the minimum charge product throughout the maneuver.

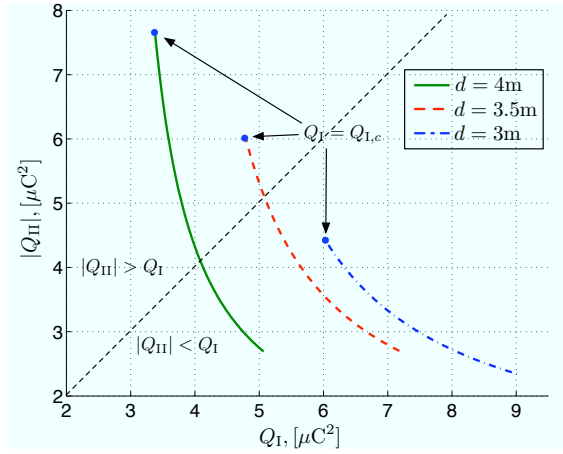
For general symmetric trajectory cases, given a value of  $d$ , there remains one degree of freedom to determine the collision avoidance trajectory. The numerical algorithm presented in the last section chooses a value of  $Q_1$  and calculates all the remaining variables. Figure 8(b) shows the value of  $|Q_{II}|$  corresponding to  $Q_1$  under different  $d$ , with all other variables the same as in Figure 8(a).

Figure 8(b) illustrates that the solution with  $|Q_{II}| < Q_1$  always exists, while the solution with  $|Q_{II}| > Q_1$  exists only when  $d > d^*$ . This agrees with the intuition that  $Q_1$  can be infinitely large to achieve the symmetric collision avoidance trajectory, but it must be greater than a certain value to ensure a collision avoidance with  $r > r_s$ . When  $d < d^*$ , the minimum acceptable value of  $Q_1$  is still greater than corresponding  $|Q_{II}|$  as predicted by Theorem 3, thus the solution with  $|Q_{II}| > Q_1$  does not exist in this situation. Another important aspect is that if  $d < d^*$ , the solution with  $Q_1 = |Q_{II}|$  is the  $L_\infty$  optimal charge solution; when  $d > d^*$ , the circular transfer orbit is the  $L_\infty$  charge optimal solution. This helps to choose a proper value of  $Q_1$  such that the maximum charge level during the whole process is minimized.

Note that the criteria in Eq. (61) has exactly the same form as Eq. (42) in Reference 15. The authors of Reference 15 assume that the two spacecraft are fully charged to get the criteria in Eq. (42). This assumption matches with the situation in Phase-I, where the two spacecraft have a constant charge product and are repelling each other. The physical meanings of the criteria in Eq. (42) in Reference 15 can be utilized here. For a given formation flying mission in which the maximum magnitude of the possible separation distance rate has been determined, Eq. (61) provides a guide to design the spacecraft charge devices such that  $Q_{1,c}$  is achievable, thus the collision can be avoided with a symmetric trajectory.



a) Circular transitional trajectory.

b) General symmetric trajectory solution,  $Q_I$ - $Q_{II}$  plane.Figure 8: Charge product values under different  $d$ .

If the maximum charge product has been specified, then Eq. (63) below tells us the maximum allowable relative velocity that guarantees the collision to be avoidable.

$$v_0 \leq \sqrt{\frac{2Q_{I,\max}k_c(m_1 + m_2)}{m_1 m_2} \frac{r_s(r_\phi - r_s)}{r_\phi(d^2 - r_s^2)}} \quad (63)$$

Note that the inequality in Eq. (63) is obtained by solving for  $v_0$  from the inequality in Eq. (61).

## VI. Numerical Simulations

A numerical iteration routine using Newton's method to solve for a symmetric patched conic section trajectory has been set up. The logic of the routine is to search an appropriate time value  $t_B$  such that the target function  $g(t_B)$  defined in Eq. (49) converges to zero, with the point  $D$  being the periapsis of Phase-II.

The following numerical simulation cases show the effectiveness of the routine in different situations. All the cases share a common set of the parameters of the two spacecraft system:

$$m_1 = m_2 = 50 \text{ kg}, \quad r_\phi = 15 \text{ m}, \quad r_s = 7 \text{ m}, \quad \gamma = 1. \quad (64)$$

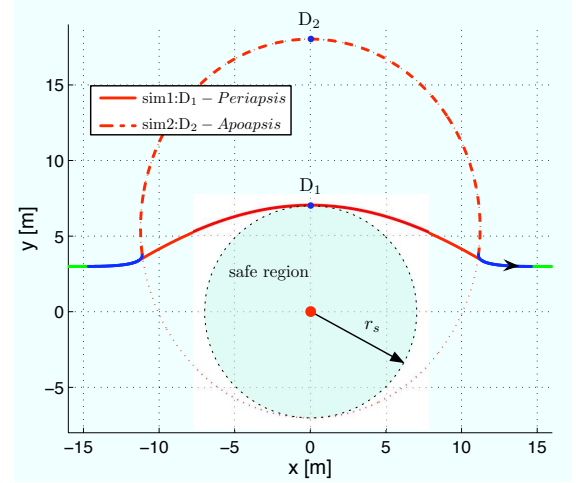
The initial inertial state vectors are also the same across all numerical studies unless specified:

$$\begin{cases} \mathbf{R}_1(t_0) = [0, 0, 0]^T \text{ m} \\ \mathbf{R}_2(t_0) = [-16, 3, 0]^T \text{ m} \end{cases} \quad \begin{cases} \dot{\mathbf{R}}_1(t_0) = [0, 0, 0]^T \text{ m/s} \\ \dot{\mathbf{R}}_2(t_0) = [0.02, 0, 0]^T \text{ m/s} \end{cases} \quad (65)$$

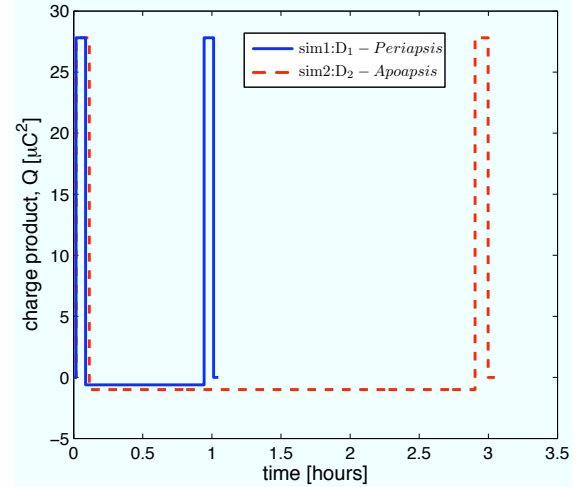
The numerical simulation integrates the fundamental equations of motion in Eq. (4) using a variable step size 4<sup>th</sup> order Runge-Kutta integrator.

### A. Ideal Conditions Examples

The phrase ‘‘ideal conditions’’ means the two spacecraft are flying in free space in a vacuum (no plasma environment) with  $\lambda_d = \infty$ . Setting the variable  $\mu_1 = -0.01 \text{ m}^3/\text{s}^2$ , the corresponding charge product is  $Q_I = 27.81 (\mu\text{C})^2$ . Figure 9 shows two simulation results under these conditions. The first trajectory (solid line) has the point  $D$  as the periapsis of Phase-II. The second trajectory (dashed line) is the case that the point  $D$  is the apoapsis of Phase-II. This can be achieved by initializing  $t_B$  to be larger than  $t_{p,1}$ , and using  $\mu_{II}^{(1)}$  instead of  $\mu_{II}^{(2)}$  in the routine. Table 1 shows some detailed results of the simulations.



a) Relative trajectories.



b) Charge product histories.

Figure 9: Idea simulation.

Table 1: Results of the ideal simulations.

	$t_B$ [s]	$r_D$ [m]	$Q_{II}$ [ $\mu\text{C}^2$ ]
sim 1	291.42	7.00	-6.480
sim 2	391.61	15.64	-1.036

In both of the two simulations the collision avoidance requirement  $r_{\min} \geq r_s$  is satisfied, and the final relative speed direction is held the same as the initial direction. The first simulation has the shorter path, though the magnitude of  $Q_{II}$  is bigger. The apoapsis case (the point  $D$  is the apoapsis of Phase-II) is a conservative trajectory far exceeding the collision avoidance requirement. Notice that a small difference in  $t_B$  results in a huge difference in the total maneuver time. The longer transition time span makes the apoapsis case much more vulnerable to disturbances.

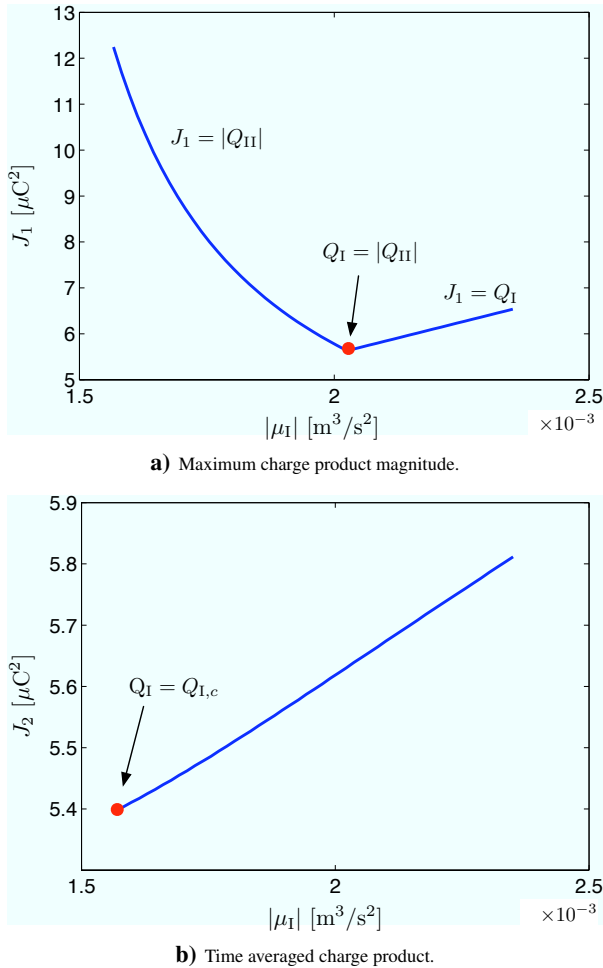


Figure 10: Charge expense history while sweeping  $\mu_I$ .

## B. Charge Expense Analysis

In these simulations the charge expense under different choices of the free variable  $\mu_I$  is analyzed. Two charge cost functions are defined as:

$$J_1 = \max(Q_I, |Q_{II}|), \quad J_2 = \frac{2t_B Q_I + t_{II} |Q_{II}|}{2t_B + t_{II}}. \quad (66)$$

Here  $J_1$  is the maximum magnitude of the charge products. This is important when the maximum vehicle voltage level is of concern.  $J_2$  is the time averaged charge product, which provides insight into the nominal charge and voltages levels. Numerical sweeps of  $|\mu_I|$  are performed using the same parameters as in Eq. (64), but with the different initial conditions:

$$\begin{cases} \mathbf{R}_1(t_0) = [0, 0, 0]^T \text{ m} \\ \mathbf{R}_2(t_0) = [-16, 6, 0]^T \text{ m} \end{cases}, \quad \begin{cases} \dot{\mathbf{R}}_1(t_0) = [0, 0, 0]^T \text{ m/s} \\ \dot{\mathbf{R}}_2(t_0) = [0.03, 0, 0]^T \text{ m/s} \end{cases} \quad (67)$$

Note that with the provided parameters and initial conditions, the condition in Theorem 3 is not satisfied, which implies the solution with  $|Q_{II}| > Q_I$  exists. Figure 10 shows the values of  $J_1$  and  $J_2$  for each value of  $|\mu_I|$ . Figure 10(a) shows that the minimum value of  $J_1$  is achieved at the marked point where  $Q_I = |Q_{II}|$ . As  $|\mu_I|$  increases, before it reaches the point where  $|Q_{II}| = Q_I$ ,  $|Q_{II}|$  dominates and  $J_1 = |Q_{II}|$ . After the marked point,  $J_1$  is linearly increasing because now  $J_1 = Q_I$  and  $Q_I$  is proportional to  $|\mu_I|$ . Figure 10(b) shows that the minimum  $J_2$  happens at the point where  $Q_I$  is minimum. This is because when  $Q_I = Q_{I,c}$ ,  $2t_B$  is about two times greater than  $t_{II}$ , and as  $|\mu_I|$  increases,  $t_B$  is increasing, and  $t_{II}$  is decreasing. So the influence of  $t_B$  dominates  $J_2$ . Thus  $J_2 \approx Q_I$  as shown in Figure 10(b).

The two plots in Figure 10 together show an example that, according to difference charge expense concerns, the “optimal” solutions can be different.

## C. Simulation With Debye Length Effect

The algorithm developed in this paper is an open loop programming algorithm, assuming that the spacecraft are flying in free space. The orbital motion and the Debye shielding effect haven't been taken into account. Figure 11 compares an ideal trajectory (dashed line) with a trajectory in the presence of the Debye shielding (solid line) under the same initial conditions. In the case that the Debye shielding is applied, the Debye length is set to be  $\lambda_d = 50$  m. This value represents the Debye length in deep space at 1 AU distance from the sun.

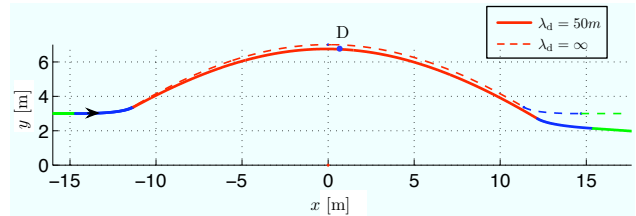


Figure 11: Relative trajectories of the two spacecraft under the condition  $\lambda_d = 50$  m.

The final velocity direction of the disturbed trajectory has an offset of  $3.98^\circ$  from the ideal trajectory. The minimum distance of the disturbed trajectory is 0.254 m or about 3.6% less than that of the ideal case  $\gamma r_s$ , due to the partial shielding of Coulomb force. The Debye length always decreases the effectiveness of the Coulomb repulsion. This effect could be compensated for with a  $\gamma > 1$  safety factor. Future work will investigate how to feedback stabilize such open-loop trajectories. A challenge here is the under-actuated nature of the Coulomb thrusting. Further, the momentum conservation makes it impossible to reverse the motion to compensate for an overshoot. Any feedback control development could try to bias the tracking errors to slightly undershoot the desired trajectory.

## VII. Conclusion

This paper proposes a symmetric 3-phase relative trajectory composed of patched conic sections as the collision avoidance trajectory. An analytical solution to circular transitional symmetric trajectory and a numerical routine to find general symmetric trajectory solutions are developed. With the presence of the Debye shielding effect, the trajectory deviates from the ideal trajectory, but only with small errors of a few percent. An issue in generating the algorithm for a multiple spacecraft formation is that increasing the number of the spacecraft would rapidly increase the complexity of the problem. But the control algorithm in this paper can be applied in a multi-spacecraft formation in the case where two spacecraft are very close and others are far away from these two spacecraft. In this case the impact from other spacecraft can be treated as disturbances. The study of the impact from other spacecraft in a formation is one direction for further study. The results in this paper can be extended to more general applications such as asymmetric flyby maneuver. The final relative velocity's direction can be controlled by changing the symmetric axis. The magnitude of the final relative velocity can be controlled by changing the energy level of Phase-III, correspondingly the properties of the Phase-III trajectory are also changed and need to be treated carefully.

## References

- R. P. Patera and G. E. Peterson, “Space Vehicle Maneuver Method to Lower Collision Risk to an Acceptable Level,” *Journal of Guidance, Control, and Dynamics*, Vol. 26, March–April 2003, pp. 233–237.
- G. L. Slater, S. M. Byram, and T. W. Williams, “Collision Avoidance for Satellites in Formation Flight,” *Journal of Guidance, Control, and Dynamics*, Vol. 29, Sept.–Oct. 2006, pp. 1140–1146.
- R. P. Patera, “Space Vehicle Conflict-Avoidance Analysis,” *Journal of Guidance, Control, and Dynamics*, Vol. 30, March–April 2007, pp. 492–498.

- <sup>4</sup>L. B. King, G. G. Parker, S. Deshmukh, and J.-H. Chong, "Spacecraft Formation-Flying using Inter-Vehicle Coulomb Forces," tech. rep., NASA/NIAC, January 2002. <http://www.niac.usra.edu>.
- <sup>5</sup>K. Torkar, W. Riedler, and C. P. Escoubet, "Active Spacecraft Potential Control for Cluster Implementation and First Results," *Annales Geophysicae*, Vol. 19, No. 10/12, 2001, pp. 1289–1302.
- <sup>6</sup>K. Torkar, W. Riedler, M. Fehringer, and et. al., "Spacecraft Potential Control aboard Equator-S as a Test for Cluster-II," *Annales Geophysicae*, Vol. 17, 1999, pp. 1582–1591.
- <sup>7</sup>K. Nishikawa and M. Wakatani, *Plasma Physics Basic Theory with Fusion Applications*. Springer, 2nd ed., 2000, pp. 56–60.
- <sup>8</sup>D. A. Gurnett and A. Bhattacharjee, *Introduction to Plasma Physics With Space and Laboratory Applications*. Cambridge University Press, 2005, pp. 7–9.
- <sup>9</sup>C. C. Romanelli, A. Natarajan, H. Schaub, G. G. Parker, and L. B. King, "Coulomb Spacecraft Voltage Study Due to Differential Orbital Perturbations," *AAS Space Flight Mechanics Meeting*, Tampa, FL, Jan. 22–26 2006. Paper No. AAS 06-123, pp. 361–380, Vol. 124 in Advances in Astronautical Sciences Society.
- <sup>10</sup>V. Lappas, C. Saaj, D. Richie, M. Peck, B. Streeman, and H. Schaub, "Spacecraft Formation Flying and Reconfiguration with Electrostatic Forces," *AAS/AIAA Space Flight Mechanics Meeting*, Sedona, AZ, Jan. 28–Feb. 1 2007. Paper AAS 07-113, pp. 217–226, Vol. 127 in Advances in Astronautical Sciences Society.
- <sup>11</sup>H. Schaub and I. I. Hussein, "Stability and Reconfiguration Analysis of a Circular Spinning 2-Craft Coulomb Tether," *IEEE Aerospace Conference*, Big Sky, MT, March 3–10 2007.
- <sup>12</sup>H. Vasavada and H. Schaub, "Analytic Solutions for Equal Mass Four-Craft Static Coulomb Formation," *Journal of the Astronautical Sciences*, Vol. 56, January–March 2008, pp. 7–40.
- <sup>13</sup>S. Wang and H. Schaub, "1-D Constrained Coulomb Structure Stabilization With Charge Saturation," *AAS/AIAA Astrodynamics Specialists Conference*, Mackinac Island, MI, Aug. 19–23 2007. Paper AAS 07–267, pp. 257–274, Vol. 129 in Advances in Astronautical Sciences Society.
- <sup>14</sup>I. I. Hussein and H. Schaub, "Stability and Control of Relative Equilibria for the Three-Spacecraft Coulomb Tether Problem," *Acta Astronautica*, Vol. 65, No. 5–6, 2009, pp. 738–754.
- <sup>15</sup>S. Wang and H. Schaub, "Spacecraft Collision Avoidance Using Coulomb Forces With Separation Distance And Rate Feedback," *AIAA Journal of Guidance, Control, and Dynamics*, Vol. 31, May–June 2008, pp. 740–750.
- <sup>16</sup>I. I. Hussein and H. Schaub, "Invariant Shape Solutions of the Spinning Three Craft Coulomb Tether Problem," *Celestial Mechanics and Dynamical Astronomy*, Vol. 96, Oct. 2006, pp. 137–157.
- <sup>17</sup>J. A. Bittencourt, *Fundamentals Of Plasma Physics*. Springer-Verlag New York, Inc., 175 Fifth Avenue, New York, NY, 2004, pp. 273–278.
- <sup>18</sup>H. Schaub, G. G. Parker, and L. B. King, "Challenges and Prospect of Coulomb Formations," *Journal of the Astronautical Sciences*, Vol. 52, Jan.–June 2004, pp. 169–193.
- <sup>19</sup>G. E. Pollock, J. W. Gangestad, and J. M. Longuski, "Charged Spacecraft Formations: A Trade Study On Coulomb And Lorentz Forces," *AAS/AIAA Spaceflight Mechanics Meeting*, Pittsburgh, PA, Aug. 10–13 2009. Paper AAS 09–389.
- <sup>20</sup>H. Schaub and J. L. Junkins, *Analytical Mechanics of Space Systems*. Reston, VA: AIAA Education Series, October 2003, pp. 404–408.